A Reaction Mechanism for the Nitrous Oxide Decomposition on Binuclear Oxygen Bridged Iron Sites in Fe-ZSM-5

ARTICLE *in* THE JOURNAL OF PHYSICAL CHEMISTRY C · FEBRUARY 2007

Impact Factor: 4.77 · DOI: 10.1021/jp065574q

4 AUTHORS, INCLUDING:

Niels Hansen
ETH Zurich
24 PUBLICATIONS **460** CITATIONS
SEE PROFILE

Andreas Heyden
University of South Carolina
65 PUBLICATIONS **2,730** CITATIONS
SEE PROFILE

Frerich J Keil
Technische Universität Hamburg-Harburg
204 PUBLICATIONS **4,839** CITATIONS
SEE PROFILE

A Reaction Mechanism for the Nitrous Oxide Decomposition on Binuclear Oxygen Bridged Iron Sites in Fe-ZSM-5

Niels Hansen,*,† Andreas Heyden,*,‡ Alexis T. Bell,*,§ and Frerich J. Keil†

Department of Chemical Engineering, Hamburg University of Technology, D-21073 Hamburg, Germany, Department of Chemistry, University of Minnesota, Minneapolis, Minnesota 55455-0431, and Department of Chemical Engineering, University of California, Berkeley, California 94720-1462

Received: August 28, 2006; In Final Form: November 8, 2006

The reaction mechanism for the decomposition of nitrous oxide (N_2O) on hydroxylated and dehydroxylated binuclear oxygen bridged extraframework iron sites in Fe-ZSM-5 has been studied using density functional theory. The results show that if two charge exchange sites in the zeolite are in close proximity, two isolated dihydroxylated iron sites readily form an oxygen bridged iron site while releasing water. Different mechanisms for N_2O decomposition were examined on these hydroxylated binuclear iron sites. The activity for the N_2O decomposition on these sites is low. At elevated temperatures, water desorbs from hydroxylated sites and N_2O is readily decomposed on dehydroxylated iron sites. The rate-limiting step in the reaction path is N_2O dissociation. The overall activity of the N_2O decomposition on binuclear iron sites is qualitatively the same as that on isolated, single iron sites reported previously by Heyden et al. (*J. Phys. Chem. B* **2005**, *109*, 1857). More important than the nuclearity of the iron site (mono- or binuclear) for the activity of Fe-ZSM-5 in N_2O decomposition is the influence of small amounts of water in the reaction system on the nature of the iron site. As in the case of isolated, single iron sites, only the dehydroxylated binuclear iron sites show a significant activity for N_2O dissociation, while the hydroxylated sites are virtually inactive.

Introduction

The application of microporous materials as catalytic hosts for transition metals has become an important area from the viewpoint of environmental catalysis.[1−3] Special attention is addressed to iron-exchanged ZSM-5 because these materials are very active for the catalytic decomposition and catalytic reduction of N_2O emitted from industrial waste streams.[4,5] The state of iron in Fe-ZSM-5 is strongly dependent on the method of iron exchange, the level of Fe exchange (i.e., the Fe/Al ratio), and the pretreatment of the as-exchanged material. It is therefore not surprising that different research groups report experimental findings, which seem inconsistent with one another concerning the nature of the active site and the rate-limiting step of the N_2O decomposition. Both mononuclear and binuclear iron sites have been proposed as the principal active site,[6−9] and either N_2O dissociation or O_2 desorption have been suggested as the rate-limiting step in the overall process of N_2O decomposition.[10−15] An extensive review on the preparation and characterization of Fe-ZSM-5 catalyst materials is given by Heijboer.[16] In this study, an effort is made to relate the methods of catalyst preparation to the iron species produced and their role in NO_x/N_2O removal and selective oxidation. A conclusion of this work is that it seems impossible at present to prepare a Fe-ZSM-5 sample that contains exclusively a single active iron species. Moreover, no single experimental technique is capable of defining the structure of active sites unambiguously.

Given the diversity of the Fe-containing sites present in Fe-ZSM-5, it seems reasonable to use theoretical methods as a complement to experimental methods in order to obtain a clearer view of what types of Fe sites might be involved in N_2O decomposition to N_2 and O_2, and the mechanism by which this process occurs. Important progress has been made recently in two comprehensive theoretical studies of the mechanism and kinetics of N_2O decomposition on isolated, single extraframework iron sites in the absence[12,13] and presence of NO.[17,18] It was found that N_2O decomposition is first order with respect to N_2O concentration and that water impurities in the gas stream have a strong inhibiting effect. The proposed reaction mechanisms together with the rate coefficients calculated for each elementary step were able to explain and reproduce various transient and steady-state experiments.

The present study is an extension of the work done by Heyden et al.[12,17] to binuclear oxygen bridged iron sites. The formation of such complexes is proposed for over-exchanged Fe-ZSM-5 prepared by the sublimation technique[19,20] as well as upon activation treatments of Fe-ZSM-5 prepared by other routes.[16,21,22] For binuclear Fe-complexes, a number of molecular active site structures have been proposed, compensating one[23] or two lattice charges.[24] This study focuses on the investigation of $Z^-[-OFeOFeO-]^{2+}Z^-$ sites (Z^- represents the charge exchange sites in the zeolite), which were proposed by Chen and Sachtler,[25] El-Malki et al.,[26] Marturano et al.,[27] Čík et al.,[28] and Starokon et al.[29] There are very few quantum chemical studies on binuclear Fe complexes serving as active site models in zeolites,[30−33] and only in the work of Yakovlev et al.[33] were parts of the zeolitic framework included in the cluster model. In the latter study several catalytic cycles of the N_2O decomposition on a binuclear Fe complex are discussed from a thermodynamic point of view. Neither activation energies nor

* Corresponding authors. E-mail: (N.H.) n.hansen@tuhh.de; (A.H.) a.heyden@gmx.net; (A.T.B.) bell@cchem.berkeley.edu.

† Department of Chemical Engineering, Hamburg University of Technology.

‡ Department of Chemistry, University of Minnesota, Minneapolis.

§ Department of Chemical Engineering, University of California, Berkeley.

10.1021/jp065574q CCC: $37.00
Published on Web 01/17/2007

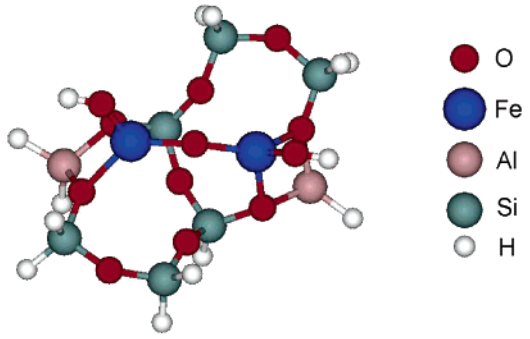

Figure 1. Active site model, $Z^-[HOFeOFeOH]^{2+}Z^-$, for the N_2O decomposition in Fe-ZSM-5.

rates of elementary reactions were reported and spin-surface crossing was not considered. It is the aim of the present study to analyze the energetics and kinetics of the N_2O decomposition on hydroxylated and dehydroxylated binuclear oxygen bridged extraframework iron sites. It is demonstrated that the formation of such complexes occurs readily if two charge exchange sites in the zeolite are in close proximity. Of particular interest was to examine whether single or bi-/oligonuclear iron sites are more active for decomposition of N_2O. In addition, we determined the rate-limiting step in the N_2O decomposition on binuclear iron sites and the order of the reaction. We illustrate how the nature of the active site and the associated reaction mechanism change with temperature. Finally, we studied the influence of antiferromagnetic coupling of the two iron centers on the reaction mechanism of the N_2O decomposition. In the present work, we introduce a detailed reaction mechanism for the N_2O decomposition on binuclear iron sites. In a companion paper, we will report the rate parameters for all elementary processes and use them to simulate the N_2O decomposition under various conditions.

Computational Details

As noted in the Introduction, this study focuses on the investigation of $Z^-[\text{-}OFeOFeO\text{-}]^{2+}Z^-$ complexes. Therefore, two Al substituted T-sites in close proximity are required to charge balance the active site. The Al distribution in Fe-ZSM-5 has been the subject of several theoretical studies using statistical methods[34−38] and quantum chemical calculations.[39−42] According to Rice et al.[37] 5T rings are the preferable exchange sites for Fe cations in Fe-ZSM-5. Goodman et al.[38] noted that the open ZSM-5 channel structure favors Al pairs that lie along one side of a channel wall rather than across a channel. Quantum chemical calculations have revealed that Al substitutes preferentially at T9 and T12 position. Combining these findings, an inter-ring bridging structure consisting of two adjoining 5T rings where in one ring the T9 and in the other ring the T12 site is substituted by Al was used in the present work as model of the catalytically active site. We note, though, that since the distribution of framework Al during zeolite synthesis may be controlled kinetically rather than energetically, as concluded by Han et al.,[43] a number of other possible binuclear structures may also be present in Fe-ZSM-5.

The catalytically active center and a portion of the zeolite framework are represented by a 34−41 atom cluster consisting of a pair of 5T rings sharing an edge (see Figure 1). All Si atoms were placed in their crystallograpic positions as reported by Olson et al.[44] The Si−O bonds not belonging to the 5T rings were replaced by terminal Si−H bonds oriented in the direction of the former Si−O bond. The Si−H bond length was set to 1.487 Å, which is the optimized bond length for SiH_4 at the B3LYP/TZVP level of theory. The resulting coordinates for the terminal H atoms were then held fixed throughout all subsequent calculations while all other coordinates were allowed to relax. The Si atoms at the T9 and T12 positions were substituted by Al atoms. The present cluster model is similar to the one of Yakovlev et al.[33] The two models differ only in the methods used to determine the fixed atom positions. Yakovlev et al.[33] first optimized the Si−H distances of the terminal hydrogen atoms for the ZH_2 model and then kept the positions of these atoms frozen in all subsequent calculations. As a result, the cluster model used in the present work resembles the crystallographic structure of ZSM-5 more closely than the cluster model used by Yakovlev et al.[33] Nevertheless, it is noted that this subtle difference in the two models is not expected to affect electronic energy differences significantly.

Calculation of the ground state energy of a binuclear metal cluster by density functional methods is complicated by the spin coupling of the unpaired electrons in the metal centers.[45−48] The spin coupling parameter J can be calculated using the original broken-symmetry approach proposed by Noodleman through the following equation:[49]

$$E_{HS} - E_{BS} = -2S_1S_2J \quad (1)$$

Here S_1 and S_2 are the total spins of the two interacting paramagnetic centers. The first energy term, E_{HS}, corresponds to the high spin solution and the second one, E_{BS}, to the broken-symmetry solution, a single-determinant wave function with $S_z = 0$ and opposite spins at the two paramagnetic centers. Equation 1 was shown to give accurate results for self-interaction free methods.[50] For DFT calculations not corrected for the self-interaction error, the following nonprojected approach was demonstrated to give accurate coupling constants.[50,51]

$$E_{HS} - E_{BS} = -(2S_1S_2 + S_2)J \quad (2)$$

Equation 2 was used in the present work to calculate coupling constants for the binuclear oxygen bridged iron site.

The representation of the open-shell low spin coupling ($M_s = 1$) of the two iron centers by a single determinant method like DFT usually gives a heavily spin contaminated wave function, which makes the results questionable especially for energetics.[52] As a consequence, it is necessary to apply a multireference method; however, this is impractical for the system sizes studied in this work. Therefore, if the reaction mechanism is not influenced by antiferromagnetic coupling it is computationally more practical to ignore the antiferromagnetic nature of the system and to perform spin-unrestricted open-shell calculations for ferromagnetically coupled high-spin states.[53] In the present work, the catalytic cycles for the decomposition of N_2O on binuclear oxygen bridged iron sites were determined using spin-unrestricted open-shell calculations for ferromagnetically coupled high spin states. For the most relevant reaction steps additional broken-symmetry calculations have been carried out to study the influence of antiferromagnetic coupling on the reaction mechanism of the N_2O decomposition and to validate the ferromagnetically coupled high-spin calculations. As mentioned above, all reported results for antiferromagnetically coupled states are subject to large spin contamination. We obtained numbers for the expectation value $\langle \hat{S}^2 \rangle$ ranging between 3.9 for ground states and 4.9 for transition states, far away from the correct value, $S(S + 1) = 0$, for a singlet state.

For the ferromagnetically coupled high spin states quantum chemical calculations of the geometry and potential energy

TABLE 1: Geometries and Imaginary Frequencies of the Transition States in N_2O Decomposition on Ferromagnetically Coupled Binuclear Oxygen Bridged Iron Sites[a]

elementary step	$R_{NN'}$ (Å)	$R_{N'O}$ (Å)	∠NN′O (deg)	ω (cm^{-1})
$Z^-[HOFeOFeOH]^{2+}(ON_2)Z^- \rightarrow Z^-[HOFeOOFeOH]^{2+}Z^- + N_2$	1.10	1.61	153.4	690*i*
$Z^-[HOFe(ON_2)\_FeOH]^{2+}Z^- \rightarrow Z^-[HOFeO\_FeOH]^{2+}Z^- + N_2$	1.14	1.38	137.4	502*i*
$Z^-[HOFeO\_(N_2O)FeOH]^{2+}Z^- \rightarrow Z^-[HOFeO\_OFeOH]^{2+}Z^- + N_2$	1.13	1.42	136.9	673*i*
$Z^-[FeOHFeOH]^{2+}(ON_2)Z^- \rightarrow Z^-[OFeOHFeOH]^{2+}Z^- + N_2$	1.11	1.51	145.0	820*i*
$Z^-[OFeOHFeOH]^{2+}(ON_2)Z^- \rightarrow Z^-[OOFeOHFeOH]^{2+}Z^- + N_2$	1.13	1.50	131.3	810*i*
$Z^-[FeOFe]^{2+}(ON_2)Z^- \rightarrow Z^-[FeOFeO]^{2+}Z^- + N_2$	1.13	1.43	136.7	619*i*
$Z^-[FeOFeO]^{2+}(ON_2)Z^- \rightarrow Z^-[OFeOFeO]^{2+}Z^- + N_2$	1.12	1.46	137.7	770*i*
$Z^-[FeOFe]^{2+}(ON_2)Z^- \rightarrow Z^-[OFeOFe]^{2+}Z^- + N_2$	1.13	1.44	136.7	650*i*
$Z^-[OFeOFe]^{2+}(ON_2)Z^- \rightarrow Z^-[OFeOFeO]^{2+}Z^- + N_2$	1.13	1.45	137.6	754*i*

[a] The connectivity of the atoms is assumed to be NN′O.

minima were performed for spin potential energy surfaces with spin multiplicity $M_S = 7$ to 11, using gradient-corrected spin density-functional theory (DFT). To represent the effects of exchange and correlation, Becke's three-parameter exchange functional[54] together with the correlation functional of Lee, Yang, and Parr (B3LYP)[55] was used with a very fine numerical grid size (m5).[56] The B3LYP functional has proven to be effective for a number of reactions involving iron oxide molecules,[57−60] leading us to conclude that a DFT-B3LYP approach can also be used successfully to investigate N_2O decomposition on binuclear oxygen bridged iron sites in Fe-ZSM-5. Basis sets at the triple-ζ level with polarization functions (TZVP) were used for all atoms including iron.[61] Electronic energy differences were found to be converged with respect to the basis set size. All calculations were carried out using the TURBOMOLE V5.7 suite of programs[62] in C_1 symmetry. Our calculations on different spin potential energy surfaces (PESs) revealed that the energy difference between different PESs is usually significant so that only energies of PES minima for the ground state are reported. Spin contamination was not observed for ground-state minimum structures. Some spin contamination was observed for transition states and minimum structures on the seam of two PESs. Nevertheless, in all cases it was still possible to distinguish clearly between states of different spin multiplicities.

Two recent DFT studies have demonstrated that the B3LYP functional gives very accurate results for the coupling constant *J* of binuclear Fe complexes in models of metalloenzymes, with four to five unpaired electrons on each cation, using directly the energies corresponding to the broken-symmetry wave function.[50,63] These results suggest that the DFT/B3LYP approach can also be used successfully to study antiferromagnetic coupling in binuclear oxygen bridged iron sites in Fe-ZSM-5. In the present study we computed broken-symmetry solutions for the most relevant reaction steps (determined from ferromagnetic DFT calculations) along the catalytic cycle to investigate the influence of antiferromagnetic coupling in binuclear oxygen bridged iron sites on the reaction mechanism. For each broken-symmetry solution, we computed the Mulliken spin densities to check whether the number of unpaired electrons was close to the formal integer value (3.5−3.7 for an Fe(II)-d^4 center and 3.8−4.1 for an Fe(III)-d^5 center).[63]

During the geometry optimizations, energies were converged to 10^{-7} Ha and the maximum norm of the Cartesian gradient to 10^{-4} Ha/bohr. Transition states were localized using a combination of interpolation and local methods. The growing-string method[64] was used in mass-weighted coordinates with a maximum of 13 to 16 nodes. After the two ends of the growing string join, the growing-string method was terminated and an approximate saddle point was obtained. To refine the position of the saddle point, the modified-dimer method[65] was employed. A gradient norm convergence criterion of 5×10^{-4} Ha/bohr was used for the transition state searches. Minimum potential energy structures on the seam of two PESs were determined with a multiplier penalty function algorithm (see Heyden et al.[12] and Heyden[66] for details). Converged minimum energy crossing point structures had a maximum energy difference between both PESs of less than 10^{-6} Ha.

Results and Discussion

The nuclearity of the active site in Fe-ZSM-5 for the decomposition of N_2O is still a matter of active debate in the literature. While it has been proposed that different preparation and pretreatment methods produce different kinds of active sites, Pirngruber et al.[22] have observed that differently prepared zeolites show qualitatively similar catalytic behavoir in N_2O decomposition. The present study supports this experimental finding by demonstrating that the overall behavoir of the N_2O decomposition on binuclear oxygen bridged iron sites does not differ considerably from that on isolated, single iron sites. In addition, we show that oxygen migration over a binuclear iron structure is not expected to be the rate-limiting step of the catalytic cycle.

In what follows, we first present calculations showing how binuclear oxygen bridged iron sites can be formed. Second, two different catalytic cycles for the N_2O decomposition on hydroxylated binuclear iron sites are presented. Third, we show how N_2O dissociates on dehydroxylated binuclear iron sites. The latter mechanism takes place at elevated temperatures after water has desorbed from the catalytic surface. Fourth, we show that the reaction mechanism for N_2O decomposition on binuclear oxygen bridged iron sites is essentially unchanged if antiferromagnetic coupling is taken into account.

In Table 1, geometries of the transition states as well as the imaginary frequencies associated with the transition state mode for the N_2O dissociation steps on the ferromagnetically coupled PES are summarized. Table 2 lists the imaginary frequencies of all other transition states on the ferromagnetically coupled PES. In Table 3, geometries and imaginary frequencies associated with the transition state mode for transition states determined with the broken-symmetry approach are presented. Coupling constants for the N_2O decomposition on $Z^-[FeOFe]^{2+}Z^-$ are summarized in Table 4. All enthalpies discussed in the text are averaged over a temperature range from 600 to 800 K.

Formation of Binuclear Iron Sites. The existence of $Z^-[Fe(OH)_2]^+$ sites in Fe-ZSM-5 prepared by solid-state exchange of H-ZSM-5 with $FeCl_3$ and by high-temperature pretreatment of Fe/Al−MFI has been demonstrated in XAFS investigations.[67,68] A recent DRIFTs study of Krishna and Makkee[69] also shows that high-temperature catalyst preparation or pretreatment leads to isolated dihydroxylated iron species $Z^-[Fe(OH)_2]^+$. Figure 2 illustrates a mechanism by which an oxygen bridged iron site of type $Z^-[HOFeOFeOH]^{2+}Z^-$ is

TABLE 2: Imaginary Frequencies of Transition States on the Ferromagnetically Coupled PES Not Involved in N_2O Dissociation

elementary step	ω (cm^{-1})
$Z^-[HOFe\_O_2FeOH]^{2+}Z^- \rightarrow Z^-[HOFe\_FeOH]^{2+}Z^- + O_2$	16*i*
$Z^-[O_2FeOHFeOH]^{2+}Z^- \rightarrow Z^-[FeOHFeOH]^{2+}Z^- + O_2$	90*i*
$Z^-[FeOFeO_2]^{2+}Z^- \rightarrow Z^-[FeOFe]^{2+}Z^- + O_2$	78*i*
$Z^-[HOFeOHFe(OH)_2]^{2+}Z^- \rightarrow Z^-[HOFeOFeOH]^{2+}(OH_2)Z^-$	1141*i*
$Z^-[HOFeOOFeOH]^{2+}Z^- \rightarrow Z^-[HOFe\_O_2FeOH]^{2+}Z^-$	118*i*
$Z^-[HOFe\_FeOH]^{2+}Z^- \rightarrow Z^-[FeOHFeOH]^{2+}Z^-$	18*i*
$Z^-[OFeOHFeOH]^{2+}Z^-\{M_S = 9\} \rightarrow Z^-[OFeOFeOH_2]^{2+}Z^-$	943*i*
$Z^-[OFeOHFeOH]^{2+}Z^-\{M_S = 11\} \rightarrow Z^-[HOFeOFeOH]^{2+}Z^-$	1291*i*
$Z^-[FeOHFeOH]^{2+}Z^- \rightarrow Z^-[FeOFeOH_2]^{2+}Z^-$	1141*i*
$Z^-[OOFeOHFeOH]^{2+}Z^- \rightarrow Z^-[O_2FeOHFeOH]^{2+}Z^-$	754*i*
$Z^-[HOFeO\_OFeOH]^{2+}Z^- \rightarrow Z^-[HOFeOOFeOH]^{2+}Z^-$	382*i*
$Z^-[HOFeO\_FeOH]^{2+}Z^- \rightarrow Z^-[HOFeOFeOH]^{2+}Z^-$	180*i*
$Z^-[OFeOFeO]^{2+}Z^- \rightarrow Z^-[FeOOFeO]^{2+}Z^-$	629*i*
$Z^-[FeOOFeO]^{2+}Z^- \rightarrow Z^-[FeO_2FeO]^{2+}Z^-$	260*i*
$Z^-[FeO_2FeO]^{2+}Z^- \rightarrow Z^-[FeOFeO_2]^{2+}Z^-$	145*i*

formed from two $Z^-[Fe(OH)_2]^+$ species while releasing water. This reaction is calculated to be endothermic with an enthalpy of reaction of $\Delta H_R = 18.8$ kcal/mol. The reaction mechanism consists of a sequence of three slightly endothermic elementary reactions, none of which has a reaction barrier larger than 10.6 kcal/mol. As a result, the overall barrier for the reaction $Z^-[HOFeOH\_HOFeOH]^{2+}Z^- \rightarrow Z^-[HOFeOFeOH]^{2+}Z^- + H_2O$ is calculated as the energy difference between $Z^-[HOFeOFeOH]^{2+}Z^- + H_2O$ and $Z^-[HOFeOH\_HOFeOH]^{2+}Z^-$, with $E^‡ = 19.2$ kcal/mol. Considering the low H_2O partial pressure in industrial exhaust streams the entropy gain in desorbing a water molecule outweighs the higher energy of the products and significant more binuclear iron species than isolated $Z^-[Fe(OH)_2]^+$ sites are present in equilibrium at low temperatures. Steady-state simulations of the catalytic surface taking into account the whole reaction network presented in this work show that the formation of $Z^-[HOFeOFeOH]^{2+}Z^-$ sites takes place already at room-temperature if two iron sites are in close proximity.

N_2O Decomposition on $Z^-[HOFeOFeOH]^{2+}Z^-$ Sites. Figure 3 illustrates a catalytic cycle for the decomposition of N_2O on $Z^-[HOFeOFeOH]^{2+}Z^-$ sites. Nitrous oxide adsorbs on $Z^-[HOFeOFeOH]^{2+}Z^-$ through the O-end with an enthalpy of adsorption of $\Delta H_{ads} = -0.8$ kcal/mol. The activation barrier for the reaction of $Z^-[HOFeOFeOH]^{2+}(ON_2)Z^-$ to form $Z^-[HOFeOOFeOH]^{2+}Z^-$ and N_2 is $E^‡ = 40.2$ kcal/mol. The peroxo structure $Z^-[HOFeOOFeOH]^{2+}Z^-$ was calculated to have a lower energy than the structure that would appear if the oxygen was deposited on top of the iron. This result is in line with DFT calculations on isolated, single iron sites conducted by Heyden et al.[12] In the latter study, it was shown that the reaction of $Z^-[Fe(OH)_2]^+(ON_2)$ to form $Z^-[OFe(OH)_2]^+$ and N_2 is endothermic, with an enthalpy of reaction of $\Delta H_R = 16.7$ kcal/mol and an activation energy of $E^‡ = 42.8$ kcal/mol on the sextet PES. In the present study an enthalpy of reaction of $\Delta H_R = 18.9$ kcal/mol and an activation energy of more than 40.0 kcal/mol has been calculated for the corresponding reaction, i.e., for $Z^-[HOFeOFeOH]^{2+}(ON_2)Z^- \rightarrow Z^-[HOFeOFeOOH]^{2+}Z^- + N_2$ (not shown in Figure 3). The formation of the peroxo structure $Z^-[HOFeOOFeOH]^{2+}Z^-$ is slightly exothermic with an enthalpy of reaction of $\Delta H_R = -1.4$ kcal/mol. From the latter structure $Z^-[HOFe\_O_2FeOH]^{2+}Z^-$ is formed by surmounting an activation barrier of $E^‡ = 6.5$ kcal/mol. This reaction is endothermic with an enthalpy of reaction of $\Delta H_R = 5.2$ kcal/mol. Molecular oxygen can desorb from $Z^-[HOFe\_O_2FeOH]^{2+}Z^-$. The O_2 desorption barrier is $E^‡ = 9.2$ kcal/mol and the enthalpy of desorption is 1.7 kcal/mol. A N_2O molecule can dissociate on each hydroxylated iron site of $Z^-[HOFe\_FeOH]^{2+}Z^-$. N_2O adsorbs from the O-end on the T9 site with an enthalpy of adsorption of $\Delta H_{ads} = -0.2$ kcal/mol. The activation energy for the reaction of $Z^-[HOFe(ON_2)\_FeOH]^{2+}Z^-$ to form $Z^-[HOFeO\_FeOH]^{2+}Z^-$ and N_2 is $E^‡ = 25.9$ kcal/mol. This reaction is exothermic by $\Delta H_R = -15.0$ kcal/mol. On the T12 site, N_2O adsorbs from the O-end with an enthalpy of adsorption of $\Delta H_{ads} = 0.2$ kcal/mol. The activation energy for the reaction, $Z^-[HOFeO\_(N_2O)FeOH]^{2+}Z^- \rightarrow Z^-[HOFeO\_OFeOH]^{2+}Z^- + N_2$, is $E^‡ = 25.0$ kcal/mol. The enthalpy of reaction of this exothermic step is $\Delta H_R = -11.9$ kcal/mol. The peroxo structure $Z^-[HOFeOOFeOH]^{2+}Z^-$ is formed from $Z^-[HOFeO\_OFeOH]^{2+}Z^-$. This exothermic reaction, $\Delta H_R = -18.5$ kcal/mol, involves surmounting a small barrier of $E^‡ = 9.4$ kcal/mol and closes the catalytic cycle on $Z^-[HOFeOOFeOH]^{2+}Z^-$ sites. An alternative path goes from $Z^-[HOFeO\_FeOH]^{2+}Z^-$ back to $Z^-[HOFeOFeOH]^{2+}Z^-$, which closes the catalytic cycle on $Z^-[HOFeOFeOH]^{2+}Z^-$ sites. The latter reaction is highly exothermic with an enthalpy of reaction of $\Delta H_R = -27.9$ kcal/mol and a very small activation energy of $E^‡ = 0.1$ kcal/mol. Because of the high activation barrier for N_2O dissociation on $Z^-[HOFeO\_FeOH]^{2+}Z^-$ compared to the formation of the oxygen bridge, $Z^-[HOFeO\_FeOH]^{2+}Z^- \rightarrow Z^-[HOFeOFeOH]^{2+}Z^-$, the latter reaction is much more likely, and hardly any $Z^-[HOFeO\_FeOH]^{2+}Z^-$ is expected to be present under reaction conditions.

An alternative cycle starting from $Z^-[HOFeOFeOH]^{2+}Z^-$ is illustrated in Figure 4. As in the previous cycle $Z^-[HOFe\_FeOH]^{2+}Z^-$ is formed. Isolated $Z^-[FeOH]^+$ sites are active in N_2O decomposition.[17] However, if such species are in close proximity they tend to form an oxygen bridged structure. The reaction $Z^-[HOFe\_FeOH]^{2+}Z^- \rightarrow Z^-[FeOHFeOH]^{2+}Z^-$ is exothermic with an enthalpy of reaction of $\Delta H_R = -10.9$ kcal/mol and a very small barrier of $E^‡ = 2.0$ kcal/mol. N_2O dissociation occurs on $Z^-[FeOHFeOH]^{2+}Z^-$ only on the dehydroxylated iron atom since the reaction barrier on the hydroxylated iron atom is considerably higher. N_2O adsorbs from the O-end with an enthalpy of adsorption of $\Delta H_{ads} = -2.2$ kcal/mol. The activation energy for the reaction $Z^-[FeOHFeOH]^{2+}(ON_2)Z^- \rightarrow Z^-[OFeOHFeOH]^{2+}Z^- + N_2$ is $E^‡ = 32.3$ kcal/mol. This reaction is exothermic with an enthalpy of reaction of $\Delta H_R = -8.4$ kcal/mol. The species $Z^-[OFeOHFeOH]^{2+}Z^-$ is more stable on the 11-et PES than on the nonet PES. A negligible spin change barrier of about $E^‡ = 1.6$ kcal/mol was found for the spin inversion process. The enthalpy of reaction is $\Delta H_R = -3.6$ kcal/mol. Because of the low barrier both structures are in equilibrium. $Z^-[OFeOHFeOH]^{2+}Z^-\{M_S = 11\}$ is a possible active site for N_2O dissociation. N_2O adsorbs from the O-end with an enthalpy of adsorption of $\Delta H_{ads} = 0.1$ kcal/mol. The activation energy for the reaction $Z^-[OFeOHFeOH]^{2+}(ON_2)Z^- \rightarrow Z^-[OOFeOHFeOH]^{2+}Z^- + N_2$ is $E^‡ = 34.7$ kcal/mol. This step is exothermic with an enthalpy of reaction of $\Delta H_R = -6.8$ kcal/mol. Diatomic oxygen can be formed from dioxo species $Z^-[OOFeOHFeOH]^{2+}Z^-$. This reaction is exothermic with an enthalpy of reaction of $\Delta H_R = -15.0$ kcal/mol and has an activation energy of $E^‡ = 11.2$ kcal/mol. Molecular oxygen desorbs readily from $Z^-[O_2FeOHFeOH]^{2+}Z^-$. The activation energy for this process is $E^‡ = 0.2$ kcal/mol; the enthalpy of reaction was calculated to be $\Delta H_R = -2.5$ kcal/mol. An alternative path goes from $Z^-[OFeOHFeOH]^{2+}Z^-\{M_S = 11\}$ to $Z^-[HOFeOFeOH]^{2+}Z^-$. This process is exothermic with an enthalpy of reaction of $\Delta H_R = -18.0$ kcal/mol and has a relatively small activation energy of $E^‡ = 6.2$ kcal/mol.

TABLE 3: Geometries and Imaginary Frequencies of Transition States for Key Reactions on the Antiferromagnetically Coupled PES[a]

elementary step	$R_{NN'}$ (Å)	$R_{N'O}$ (Å)	∠NN′O (deg)	ω (cm^{-1})
$Z^-[FeOFe]^{2+}(ON_2)Z^- \rightarrow Z^-[FeOFeO]^{2+}Z^- + N_2$	1.13	1.41	136.6	635*i*
$Z^-[FeOFeO]^{2+}(ON_2)Z^- \rightarrow Z^-[OFeOFeO]^{2+}Z^- + N_2$	1.13	1.46	137.0	756*i*
$Z^-[OFeOFeO]^{2+}Z^- \rightarrow Z^-[FeOOFeO]^{2+}Z^-$				745*i*
$Z^-[FeOOFeO]^{2+}Z^- \rightarrow Z^-[FeO_2FeO]^{2+}Z^-$				335*i*
$Z^-[FeO_2FeO]^{2+}Z^- \rightarrow Z^-[FeOFeO_2]^{2+}Z^-$				409*i*
$Z^-[FeOFeO_2]^{2+}Z^- \rightarrow Z^-[FeOFe]^{2+}Z^- + O_2$				108*i*

[a] The connectivity of the atoms is assumed to be NN′O.

TABLE 4: Fe−Fe Distances and Fe−O−Fe Bond Angles for Antiferromagnetically Coupled Iron Atoms, Energy Differences between the Ferromagnetic and Antiferromagnetic PES, and Coupling Constants for $Z^-[HOFeOFeOH]^{2+}Z^-$ and Dehydroxylated Sites

	R_{FeFe} (Å)	∠FeOFe (deg)	$E_{HS} - E_{BS}$ (kcal/mol)	J (cm^{-1})
$Z^-[HOFeOFeOH]^{2+}Z^-$	3.55	158.2	6.8	−157.5
$Z^-[FeOFe]^{2+}Z^-$	3.07	117.7	4.1	−143.4
$Z^-[FeOFe]^{2+}(ON_2)Z^-$	3.11	119.2	3.9	−138.1
TS 1	3.26	129.5	5.5	−194.1
$Z^-[FeOFeO]^{2+}Z^-$	3.20	128.3	2.7	−95.5
$Z^-[FeOFeO]^{2+}(ON_2)Z^-$	3.23	128.9	2.4	−82.7
TS 2	3.40	123.2	2.5	−87.2
$Z^-[OFeOFeO]^{2+}Z^-$	3.26	133.6	1.8	−62.2
TS 3	3.55	136.4	−2.0	68.7
$Z^-[FeOOFeO]^{2+}Z^-$	3.76		0.1	−2.5
TS 4	4.40		−0.1	2.1
$Z^-[FeO_2FeO]^{2+}Z^-$	3.66		−0.1	3.4
TS 5	3.57	132.4	3.2	−110.9
$Z^-[FeOFeO_2]^{2+}Z^-\{M_s = 1\}$	3.30	133.0	5.5	−194.0
SC	3.33	135.1	5.2	−182.4
$Z^-[FeOFeO_2]^{2+}Z^-\{M_s = 3\}$	3.28	131.7	5.5	−128.7
TS 6	3.17	123.8	4.1	−95.7

[a] The coupling constants were calculated using the nonprojected approach [eq 2]. Transition states connecting the minima are denoted as TS, the minimum on the seam of two potential energy surfaces is denoted as SC.

As a result, this reaction is more likely to occur than the N_2O dissociation on $Z^-[OFeOHFeOH]^{2+}Z^-\{M_S = 11\}$.

To conclude, owing to the high activation energy for the reaction $Z^-[HOFeOFeOH]^{2+}Z^- + N_2O \rightarrow Z^-[HOFeOOFeOH]^{2+}Z^- + N_2$, both catalytic cycles presented show only a minor activity in N_2O decomposition. This result is in agreement with a recent theoretical study of isolated, single iron sites reported by Heyden et al.[12] In that study an activation energy of 41.5 kcal/mol was calculated for the first dissociation of N_2O on $Z^-[Fe(OH)_2]^+$ sites. A value only sligthly larger than the activation energy calculated for the dissociation of N_2O on $Z^-[HOFeOFeOH]^{2+}Z^-$ sites (37.7 kcal/mol). By contrast, Yakovlev et al.[33] concluded from quantum chemical calculations on a similar active site model that $Z^-[HOFeOFeOH]^{2+}Z^-$ species are active for the decomposition of N_2O. However, this conclusion is based entirely on thermodynamic aspects; no transition states were calculated in the work of Yakovlev et al.[33] In addition, the dissociation of N_2O on $Z^-[HOFeOFeOH]^{2+}Z^-$ sites to form $Z^-[HOOFeOFeOH]^{2+}Z^-$ species was calculated to be exothermic by −11.9 kcal/mol by Yakovlev et al.[33] compared to +16.7 kcal/mol in the present study. This difference can be attributed to differences in the density functionals and the basis sets used in these two studies and to the failure to account for spin surface crossing in the work of Yakovlev et al.[33] In the latter study all geometry optimizations were carried out in the local spin density approximation (LSDA) using Slater exchange[70] and Vosko−Wilk−Nusair correlation functionals.[71] At the LSDA geometry the energy was computed at the GGA level using the exchange-correlation functional of Perdew and Wang.[72] As a consequence, the ground state of $Z^-[HOFeOFeOH]^{2+}Z^-$ lies on the nonet PES while in the present work it lies on the 11-et PES. Furthermore, in the study of Yakovlev et al.[33] spin transitions along the reaction path were not considered so that all calculations with an even number of electrons were carried out on the nonet PES.

N_2O Decomposition on $Z^-[FeOFe]^{2+}Z^-$ Sites. Figure 5 illustrates the catalytic cycle on $Z^-[FeOFe]^{2+}Z^-$ sites. From $Z^-[OFeOHFeOH]^{2+}Z^-\{M_S = 9\}$ water can desorb and $Z^-[OFeOFe]^{2+}Z^-$ is formed. This process is endothermic. The overall barrier is determined by the energy difference between $Z^-[OFeOFe]^{2+}Z^-$ and $Z^-[OFeOHFeOH]^{2+}Z^-\{M_S = 9\}$ ($E^‡ = 21.5$ kcal/mol). Furthermore, water can desorb from $Z^-[FeOHFeOH]^{2+}Z^-$. This process is endothermic with an enthalpy of reaction of $\Delta H_R = 21.6$ kcal/mol. The overall barrier is determined by the energy difference between $Z^-[FeOFe]^{2+}Z^-$ and $Z^-[FeOHFeOH]^{2+}Z^-$ ($E^‡ = 22.8$ kcal/mol). Both processes are expected to occur at elevated temperatures when the entropy gain in desorbing H_2O outweighs the enthalpy term.

The fully dehydroxylated site $Z^-[FeOFe]^{2+}Z^-$ is active for N_2O decomposition, and hence in what follows we will only discuss the reaction path from $Z^-[FeOFe]^{2+}Z^-$ to $Z^-[OFeOFeO]^{2+}Z^-$ via $Z^-[FeOFeO]^{2+}Z^-$. The path via $Z^-[OFeOFe]^{2+}Z^-$ is very similar. N_2O adsorbs on $Z^-[FeOFe]^{2+}Z^-$ through the O-end with an enthalpy of adsorption of $\Delta H_{ads} = -2.7$ kcal/mol. The activation barrier for the reaction of $Z^-[FeOFe]^{2+}(ON_2)Z^-$ to form $Z^-[FeOFeO]^{2+}Z^-$ and N_2 is $E^‡ = 25.6$ kcal/mol. With respect to the gas phase, the latter reaction has an activation energy of 21.0 kcal/mol. This is slightly lower than the activation barrier calculated by Heyden et al.[12] for the N_2O decomposition on $Z^-[FeO]^+$ sites to form $Z^-[OFeO]^+$ species ($E^‡ = 24.3$ kcal/mol on PES with $M_S = 6$). The enthalpy of reaction for $Z^-[FeOFe]^{2+}(ON_2)Z^- \rightarrow Z^-[FeOFeO]^{2+}Z^- + N_2$ is $\Delta H_R = -12.6$ kcal/mol. The structure $Z^-[FeOFeO]^{2+}Z^-$ is an active site for N_2O decomposition. N_2O adsorbs through the O-end on the unoccupied Fe atom with an enthalpy of adsorption of $\Delta H_{ads} = -3.6$ kcal/mol. The activation energy for the reaction $Z^-[FeOFeO]^{2+}(ON_2)Z^- \rightarrow Z^-[OFeOFeO]^{2+}Z^- + N_2$ is $E^‡ = 30.1$ kcal/mol. With respect to the gas phase the latter reaction has an activation energy of 24.8 kcal/mol. The activation energy for depositing two oxygen atoms on the same iron atom was calculated to be $E^‡ = 42.4$ kcal/mol with respect to the gas phase, i.e., with respect to $Z^-[FeOFeO]^{2+}Z^-$. Therefore, the dissociation of two N_2O molecules on the same iron atom is very unlikely to occur. This result is in line with the two recent DFT studies on isolated, single iron sites.[12,17] For N_2O dissociation on $Z^-[OFeOH]^+$, we calculated an activation energy of 43 kcal/mol with respect to the gas-phase making this step unlikely to occur except at elevated temperatures.[17] In contrast, the N_2O dissociation barrier on $Z^-[OFeO]^+$ and $Z^-[FeO_2]^+$ sites was previously calculated to be only 12.0 kcal/mol and 17.3 kcal/mol, respectively.[12] The reason that the N_2O dissociation barrier on $Z^-[OFeOH]^+$ is significantly higher than on $Z^-[OFeO]^+$ or $Z^-[FeO_2]^+$ is that a superoxide species (O_2^-)

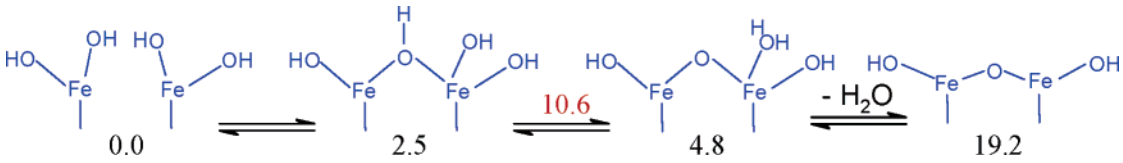

Figure 2. Formation of a binuclear oxygen bridged iron site from two dihydroxylated single iron sites. All energies are zero-point corrected, in kcal/mol and with reference to $Z^-[HOFeOH\_HOFeOH]^{2+}Z^-$ with the appropriate amounts of H_2O. Energies of potential energy minima are in black. Energies of transition states are in red. Structures in blue are on the ferromagnetically coupled PES with $M_S = 11$. The left Fe atom in each structure represents the T9 site, the right Fe atom represents the T12 site.

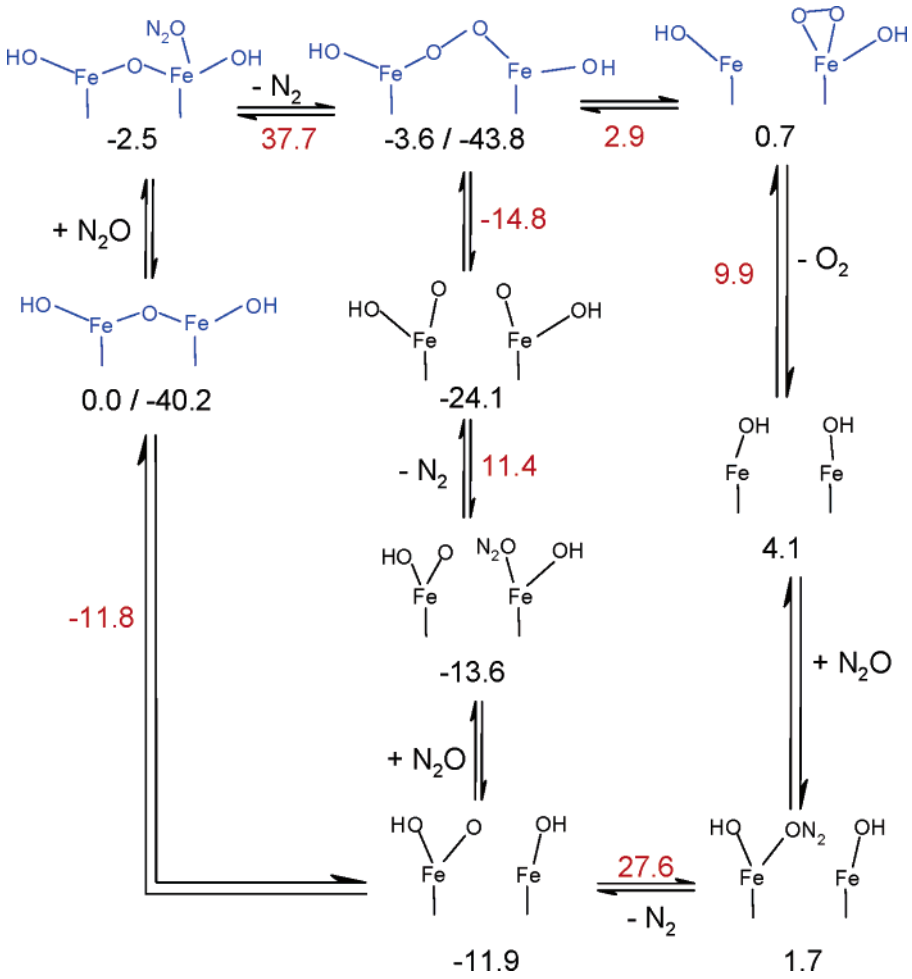

Figure 3. Catalytic cycle of the N_2O dissociation on $Z^-[HOFeOFeOH]^{2+}Z^-$ sites. All energies are zero-point corrected, in kcal/mol and with reference to $Z^-[HOFeOFeOH]^{2+}Z^-$ with the appropriate amounts of N_2O, N_2, and O_2. Energies of potential energy minima are in black. Energies of transition states are in red. Black structures are on the ferromagnetically coupled PES with $M_S = 9$. Structures in blue are on the PES with $M_S = 11$. Multiple numbers under a PES minimum structure correspond to different catalytic cycles. The left Fe atom in each structure represents the T9 site, the right Fe atom represents the T12 site.

cannot be formed on $Z^-[OFeOH]^+$ before the third oxygen atom is deposited on the iron atom as is possible on $Z^-[OFeO]^+$ or $Z^-[FeO_2]^+$ sites. Likewise, on $Z^-[FeOFeO]^{2+}Z^-$, a superoxide species cannot be formed before the third oxygen atom is deposited on the iron. This also explains why larger iron–oxo clusters are observed to be significantly less active for the dissociation of N_2O.[7,22] Here, an oxygen atom has to be deposited on an iron atom similar to an iron atom in $Z^-[OFeOFeO]^{2+}Z^-$.

The enthalpy of the reaction, $Z^-[FeOFeO]^{2+}(ON_2)Z^- \rightarrow Z^-[OFeOFeO]^{2+}Z^- + N_2$, is $\Delta H_R = -5.4$ kcal/mol. For molecular oxygen to desorb from $Z^-[OFeOFeO]^{2+}Z^-$ an oxygen atom has to migrate from one iron atom to the other. This migration proceeds via a peroxo structure $Z^-[FeOOFeO]^{2+}Z^-$. The activation energy for this process was calculated to be $E^‡ = 27.3$ kcal/mol. The reaction is endothermic with an enthalpy of reaction of $\Delta H_R = 8.3$ kcal/mol. A superoxide $Z^-[FeOFeO_2]^{2+}Z^-$ is formed from the peroxo structure $Z^-[FeOOFeO]^{2+}Z^-$ via a stable intermediate $Z^-[FeO_2FeO]^{2+}Z^-$. For the reaction, $Z^-[FeOOFeO]^{2+}Z^- \rightarrow Z^-[FeO_2FeO]^{2+}Z^-$, we calculated an activation energy of $E^‡ = 6.2$ kcal/mol. This process is exothermic with $\Delta H_R = -5.3$ kcal/mol. An activation energy of $E^‡ = 25.3$ kcal/mol was calculated for the reaction $Z^-[FeO_2FeO]^{2+}Z^-$ to form the superoxide $Z^-[FeOFeO_2]^{2+}Z^-$. This reaction is exothermic with an enthalpy of reaction of $\Delta H_R = -19.4$ kcal/mol. The latter structure is more stable on the 11-et PES than on the nonet PES. A small spin change barrier of $E^‡ = 7.6$ kcal/mol was found for the spin inversion process. The enthalpy of reaction is $\Delta H_R = -4.8$ kcal/mol. Because of the low activation energy $Z^-[FeOFeO_2]^{2+}Z^-\{M_S = 9\}$ and $Z^-[FeOFeO_2]^{2+}Z^-\{M_S = 11\}$ are in equilibrium. Molecular oxygen can desorb from $Z^-[FeOFeO_2]^{2+}Z^-\{M_S =$

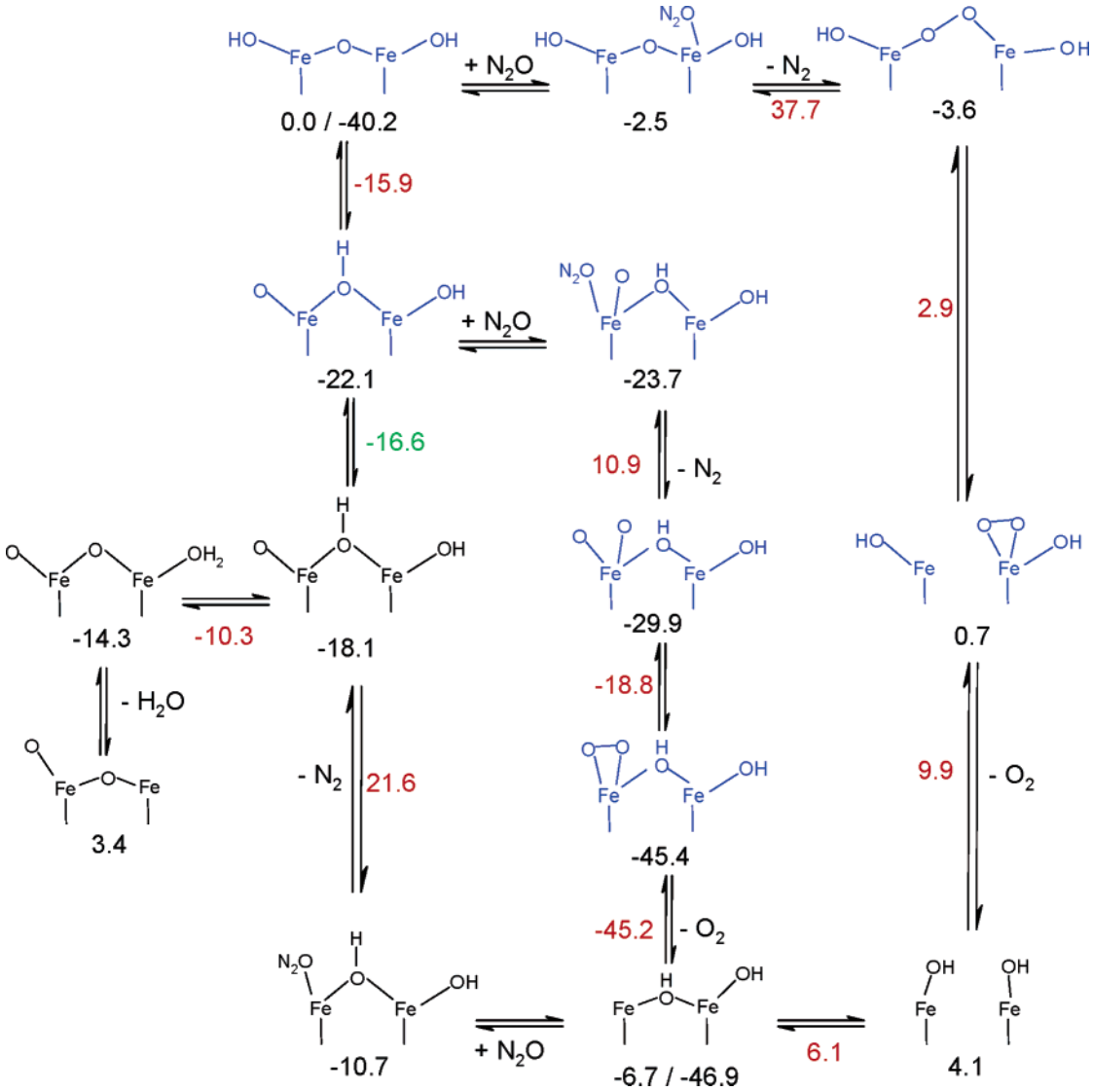

Figure 4. Alternative catalytic cycle of the N_2O dissociation on $Z^-[HOFeOFeOH]^{2+}Z^-$ sites. All energies are zero-point corrected, in kcal/mol and with reference to $Z^-[HOFeOFeOH]^{2+}Z^-$ with the appropriate amounts of N_2O, N_2, O_2, and H_2O. Energies of potential energy minima are in black. Energies of transition states are in red. Energies of minima on the seam of two PESs are in green. Black structures are on the ferromagnetically coupled PES with $M_S = 9$. Structures in blue are on the PES with $M_S = 11$. Multiple numbers under a PES minimum structure correspond to different catalytic cycles. The left Fe atom in each structure represents the T9 site, the right Fe atom represents the T12 site.

11}. The O_2 desorption barrier is $E^{\ddagger} = 8.1$ kcal/mol and the enthalpy of desorption $\Delta H_{des} = 7.1$ kcal/mol. As in all catalytic cycles reported in this study O_2 desorption is fast and, hence, oxygen inhibition is not projected to occur.

This conclusion differs from that of Kiwi-Minsker et al.,[73] who have reported that the steady-state rate of N_2O decomposition on very low Fe-content Fe-ZSM-5 is zero-order at temperatures below 600 K, and have drawn from this observation that O_2 desorption is rate-limiting. We have shown previously that this experimental observation can be explained theoretically for isolated iron sites in Fe-ZSM-5. In this case, the second N_2O dissociation step is rate-limiting at low temperatures[13] and the presence of small amounts of NO results in N_2O reaction orders of 0.1.[17,66] However, for binuclear oxygen bridged Fe sites, such as would be found in highly exchanged Fe-ZSM-5 (Fe/Al $\approx$ 1.0), the rate of the second N_2O dissociation step is rapid relative to the first, so that zero-order kinetics in N_2O should not be observed.

To conclude, the rate-limiting step along the catalytic cycle on $Z^-[FeOFe]^{2+}Z^-$ is the first N_2O dissociation step, explaining the observed first-order kinetic in N_2O partial pressure. The barrier heights with respect to the gas phase for the two successive N_2O dissociation steps are 21.0 and 24.8 kcal/mol, respectively. For isolated, single iron sites Heyden et al.[12] calculated activation energies of 24.0 and 17.3 kcal/mol, respectively. For oxygen migration to be rate-limiting on binuclear iron sites the activation energy for this process would need to be about 50 kcal/mol. Only then would $Z^-[OFeOFeO]^{2+}Z^-$ become an abundant surface intermediate and oxygen migration would become a rate-limiting step in the overall reaction network presented in the present work. The difference between this hypothetical value and the one calculated in the present work (27.3 kcal/mol) is about 22 kcal/mol, which is much larger than the error inherent in the calculation of transition states using DFT-B3LYP. Therefore, the overall steady-state behavior of N_2O decomposition on binuclear iron sites is qualitatively the same as on isolated, single iron sites. The N_2O decomposition activity of Fe-ZSM-5 is affected less by the nuclearity (mono- or binuclear) of the active iron sites than by the presence of H_2O impurities in the reaction system.

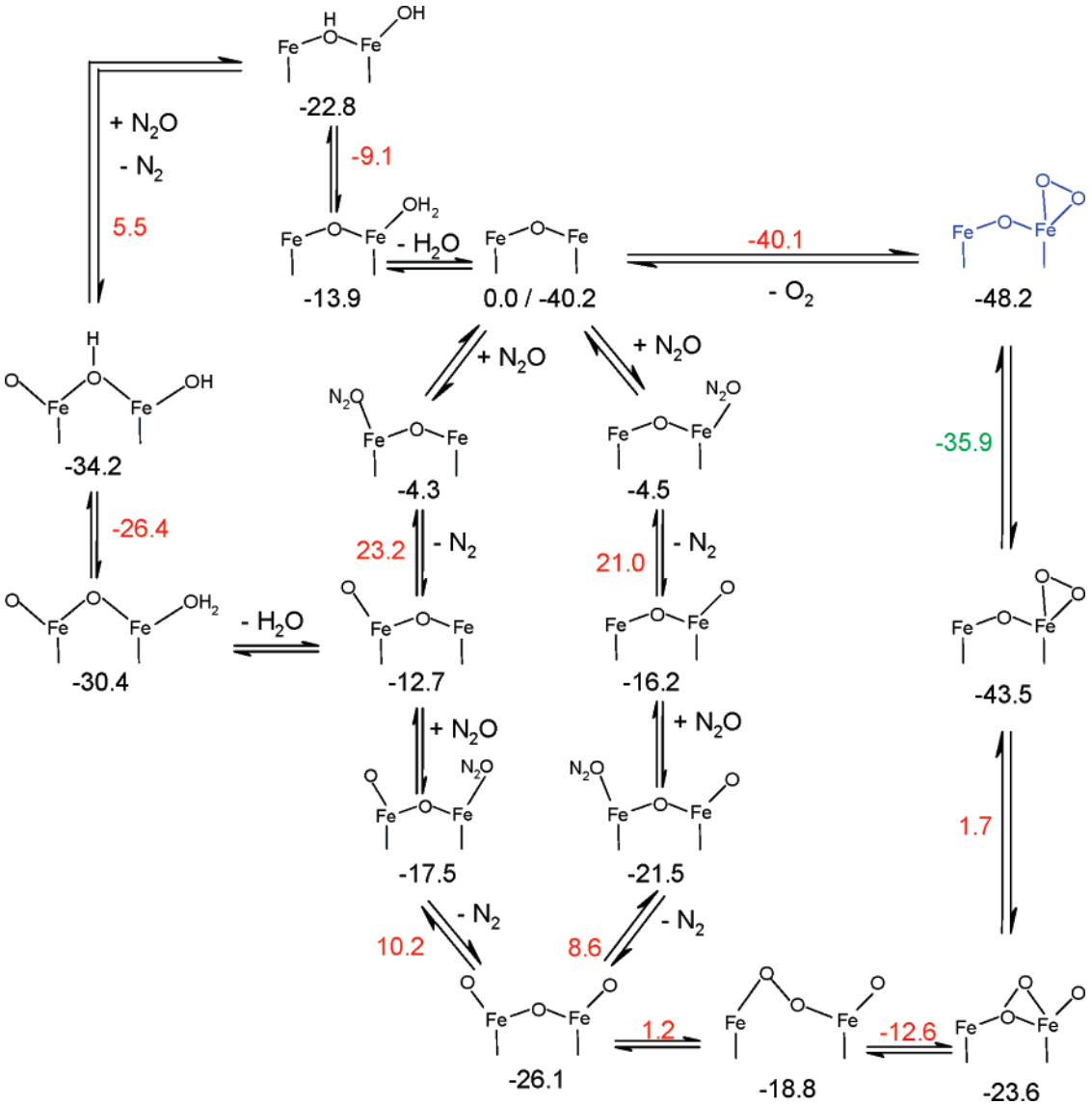

Figure 5. Catalytic cycle of the N_2O dissociation on $Z^-[FeOFe]^{2+}Z^-$ sites. All energies are zero-point corrected, in kcal/mol and with reference to $Z^-[FeOFe]^{2+}Z^-$ with the appropriate amounts of N_2O, N_2, O_2, and H_2O. Energies of potential energy minima are in black. Energies of transition states are in red. Energies of minima on the seam of two PESs are in green. Black structures are on the ferromagnetically coupled PES with $M_S = 9$. Structures in blue are on the PES with $M_S = 11$. The left Fe atom in each structure represents the T9 site; the right Fe atom represents the T12 site.

As in the case of isolated, single iron sites, only fully dehydroxylated binuclear iron sites show a significant activity for N_2O dissociation.

Effect of Antiferromagnetic Coupling. Figure 6 illustrates the energy splitting between the ferromagnetic and antiferromagnetic PES for the N_2O decomposition on $Z^-[FeOFe]^{2+}Z^-$ sites. The energy difference between the two surfaces is calculated to be 4.1 kcal/mol for $Z^-[FeOFe]^{2+}Z^-$ and 3.9 kcal/mol for the N_2O adsorbed state. After passing the first transition state where the energy difference is 5.5 kcal/mol, the difference decreases to 2.7 kcal/mol for $Z^-[FeOFeO]^{2+}Z^-$ and 2.4 kcal/mol for the N_2O adsorbed state, consistent with a larger Fe−Fe distance. The influence of antiferromagnetic coupling on the activation energies is small. For the first transition state along the catalytic cycle the activation energy is 23.9 kcal/mol on the antiferromagnetic PES and 25.5 kcal/mol on the ferromagnetic PES. For the second transition state, the activation energies are 30.0 and 30.1 kcal/mol, respectively. These differences are smaller than the error inherent in the determination of transition states using DFT/B3LYP (in particular for the broken symmetry calculations). For the reaction $Z^-[OFeOFeO]^{2+}Z^- \rightarrow Z^-[FeOOFeO]^{2+}Z^-$ the antiferromagnetic state was calculated to be higher in energy by 2 kcal/mol. As a consequence the activation energy on the antiferromagnetic PES ($E^{\ddagger} = 31.1$ kcal/mol) is 3.8 kcal/mol higher than on the ferromagnetic PES ($E^{\ddagger} = 27.3$ kcal/mol). For the peroxo structure $Z^-[FeOOFeO]^{2+}Z^-$ and the intermediate $Z^-[FeO_2FeO]^{2+}Z^-$ antiferromagnetic coupling was found to be very weak, because of the larger Fe−Fe distance. For the reaction $Z^-[FeO_2FeO]^{2+}Z^- \rightarrow Z^-[FeOFeO_2]^{2+}Z^-$ we calculated a energy difference between both PES of 3.2 kcal/mol for the transition state and 5.5 kcal/mol for the superoxide. For molecular oxygen to desorb in its ground state (a triplet $^3\Sigma_g^-$) a surface crossing from the antiferromagnetic singlet to the antiferromagnetic triplet surface has to occur. The barrier for this process was calculated to be 7.9 kcal/mol. The energy difference between both PES at the crossing point is 5.2 kcal/mol. As on the ferromagnetic PES $Z^-[FeOFeO_2]^{2+}Z^-$ is more stable in the higher spin state. The energy difference between the ferromagnetic and the antiferromagnetic PES is 5.5 kcal/mol. The O_2 desorption barrier was calculated to be 9.5 kcal/

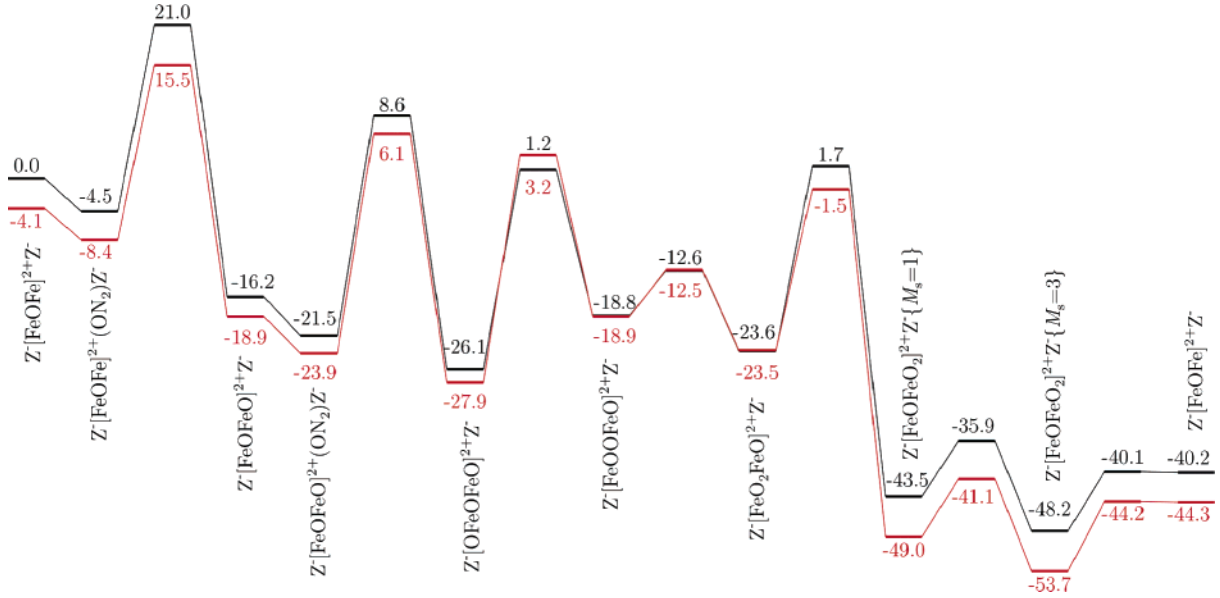

Figure 6. Reaction energy diagram of the nitrous oxide decomposition on dehydroxylated binuclear iron sites for ferromagnetically coupled high spin states (black curve) and antiferromagnetically coupled broken-symmetry states (red curve). All energies are zero-point corrected, in kcal/mol and with reference to $Z^-[FeOFe]^{2+}Z^-$ with the appropriate amounts of N_2O, N_2, and O_2. Black numbers correspond to the ferromagnetically coupled states; the energies are the same as in Figure 5. Red numbers correspond to the antiferromagnetically coupled states.

mol. The coupling constants along the catalytic cycle calculated using eq 2 are in the range from +3 to −190 cm^{-1} (see Table 4), which are common values for oxo-bridged diiron complexes in biochemistry.[74]

It can be concluded that antiferromagnetic coupling does not affect the main mechanistic aspects of the catalytic cycle such as the rate-limiting step and the approximate height of the reaction barriers. However, the overall activity of the catalytic cycle is mainly controlled by the fractions of the active sites $Z^-[FeOFe]^{2+}Z^-$, $Z^-[FeOFeO]^{2+}Z^-$, and $Z^-[OFeOFe]^{2+}Z^-$. The formation of these active sites requires the desorption of water from the inactive species $Z^-[HOFeOFeOH]^{2+}Z^-$, which predominate at low temperatures. The energy difference between the ferromagnetic and the antiferromagnetic PES for $Z^-[HOFeOFeOH]^{2+}Z^-$ was calculated to be 6.8 kcal/mol. This relatively large value shows that the strength of antiferromagnetic coupling does not depend exclusively on the Fe−Fe distance but also on the angle formed by the two iron ions and the bridging group.[74,75] The magnetic coupling is strongest for Fe−O−Fe bond angles between 120 and 180°, and decreases considerably for lower bond angles (e.g., 90°).[75] For $Z^-[HOFeOFeOH]^{2+}Z^-$ the bond angle was calculated to be 158.2°, a value much larger than the bond angles for the dehydroxylated structures (see Table 4). As a result the energy difference between the inactive $Z^-[HOFeOFeOH]^{2+}Z^-$ site and the active dehydroxylated sites is slightly larger on the antiferromagnetic than on the ferromagnetic PES. Even though this observation suggests that antiferromagnetic coupling slightly reduces the overall activity of diiron sites the effect of antiferromagnetic coupling on the reaction mechanism is small and will be quantified in a companion paper, reporting simulations of the kinetics of N_2O decomposition.

Conclusions

Three catalytic cycles for the N_2O decomposition on binuclear oxygen bridged extraframework iron sites in Fe-ZSM-5 have been investigated using density functional theory. At low temperatures the hydroxylated iron site, $Z^-[HOFeOFeOH]^{2+}Z^-$, is projected to dominate the catalytic surface. This site shows a low activity for N_2O decomposition. At higher temperatures water can desorb, and N_2O decomposition on $Z^-[FeOFe]^{2+}Z^-$ becomes the slow process in the overall kinetic. On this site N_2O decomposition deposits an oxygen atom on each iron atom, followed by subsequent oxygen atom recombination and desorption of O_2. This sequence is favored over decomposition of two N_2O molecules occurring on the same iron atom. In all of the catalytic cycles examined in this work, oxygen desorption was found to be fast and N_2O decomposition was found to be first order with respect to N_2O partial pressure. Therefore, there are many qualitative similarities between the mechanisms of N_2O decomposition on single iron sites reported by Heyden et al.[12] and that on binuclear oxygen bridged iron sites presented in the present work. Both type of sites are poisoned by small amounts of water. As a result, the nuclearity (mono- or binuclear iron site) of the catalytically active site for N_2O decomposition appears to be less important than catalyst poisoning by traces of water in the gas streams. Antiferromagnetic coupling was shown to have no effect on the reaction mechanism.

Acknowledgment. The authors would like to thank Dr. Jens Döbler, Dr. Bernd Kallies, and Dr. Uwe Huniar for support with the TURBOMOLE V5.7 software package. Computations were carried out at the "Norddeutscher Verbund für Hoch- und Höchstleistungsrechnen" (HLRN) on an IBM p690-Cluster. The present work was supported by the "Deutsche Forschungsgemeinschaft" (DFG) (German National Science Foundation) in priority program SPP 1155, the "Fonds der chemischen Industrie", the Methane Conversion Cooperative funded by BP, and the Max-Buchner Forschungsstiftung.

References and Notes

(1) Sachtler, W. M. H. *Acc. Chem. Res.* **1993**, *26*, 383.
(2) Kapteijn, F.; Rodriguez-Mirasol, J.; Moulijn, J. A. *Appl. Catal. B* **1996**, *9*, 25.
(3) Weitkamp, J., Puppe, L., Eds. *Catalysis and Zeolites, Fundamentals and Applications*; Springer: Berlin, 1999.
(4) Panov, G. I.; Sobolev, V. I.; Kharitonov, A. S. *J. Mol. Catal.* **1990**, *61*, 85.
(5) Pérez-Ramírez, J.; Kapteijn, F.; Mul, G.; Xu, X.; Moulijn, J. A. *Catal. Today* **2002**, *76*, 55.

(6) Wood, B. R.; Reimer, J. A.; Bell, A. T.; Janicke, M. T.; Ott, K. C. *J. Catal.* **2004**, *224*, 148.
(7) Berlier, G.; Ricchiardi, G.; Bordiga, S.; Zecchina, A. *J. Catal.*. **2005**, *229*, 127.
(8) Pérez-Ramírez, J. *J. Catal.* **2004**, *227*, 512.
(9) Nobukawa, T.; Yoshida, M.; Okumura, K.; Tomishige, K.; Kunimori, K. *J. Catal.* **2005**, *229*, 374.
(10) Kapteijn, F.; Marbán, G.; Rodriguez-Mirasol, J.; Moulijn, J. A. *J. Catal.* **1997**, *167*, 256.
(11) Sang, C.; Kim, B. H.; Lund, C. R. F. *J. Phys. Chem. B* **2005**, *109*, 2295.
(12) Heyden, A.; Peters, B.; Bell, A. T.; Keil, F. J. *J. Phys. Chem. B* **2005**, *109*, 1857.
(13) Heyden, A.; Bell, A. T.; Keil, F. J. *J. Catal.* **2005**, *233*, 26.
(14) Bulushev, D. A.; Kiwi-Minsker, L.; Renken, A. *J. Catal.* **2004**, *222*, 389.
(15) Sun, K.; Xia, H.; Hensen, E.; van Santen, R.; Li, C. *J. Catal.* **2006**, *238*, 186.
(16) Heijboer, W. M. New frontiers in X-ray spectroscopy of Fe-ZSM-5. Ph.D. Thesis, Utrecht University 2005.
(17) Heyden, A.; Hansen, N.; Bell, A. T.; Keil, F. J. *J. Phys. Chem. B* **2006**, *110*, 17096.
(18) Heyden, A.; Hansen, N.; Bell, A. T.; Keil, F. J. Manuscript in preparation.
(19) Marturano, P.; Drozdová, L.; Kogelbauer, A.; Prins, R. *J. Catal.* **2000**, *192*, 236.
(20) Battiston, A. A.; Bitter, J. H.; de Groot, F. M. F.; Overweg, A. R.; Stephan, O.; van Bokhoven, J. A.; Kooyman, P. J.; van der Spek, C.; Vankó, G.; Koningsberger, D. C. *J. Catal.* **2003**, *213*, 251.
(21) Kiwi-Minsker, L.; Bulushev, D. A.; Renken, A. *J. Catal.* **2003,** *219*, 273.
(22) Pirngruber, G. D.; Luechinger, M.; Roy, P. K.; Cecchetto, A.; Smirniotis, P. *J. Catal.* **2004**, *224*, 429.
(23) Dubkov, K. A.; Ovanesyan, N. S.; Shteinman, A. A.; Starokon, E. V.; Panov, G. I. *J. Catal.* **2002**, *207*, 341.
(24) Battiston, A. A.; Bitter, J. H.; Heijboer, W. M.; de Groot, F. M. F.; Koningsberger, D. C. *J. Catal.* **2003**, *215*, 279.
(25) Chen, H. Y.; Sachtler, W. H. M.; *Catal. Today* **1998**, *42*, 73.
(26) El-Malki, El-M.; van Santen, R. A.; Sachtler, W. M. H. *J. Phys. Chem. B* **1999**, *103*, 4611.
(27) Marturano, P.; Drozdová, L.; Pirngruber, G. D.; Kogelbauer, A.; Prins, R. *Phys. Chem. Chem. Phys.* **2001**, *3*, 5585.
(28) Čík, G.; Hubinová, M.; Šeršen, F.; Brezová, V. *Collect. Czech. Chem. Commun.* **2002**, *67*, 1743.
(29) Starokon, E. V.; Dubkov, K. A.; Pirutko, L. V.; Panov, G. I. *Top. Catal.* **2003**, *23*, 137.
(30) Filatov, M. J.; Pelmenschikov, A. G.; Zhidomirov, G. M. *J. Mol. Catal.* **1993**, *80*, 243.
(31) Arbuznikov, A. V.; Zhidomirov, G. M. *Catal. Lett.* **1996**, *40*, 17.
(32) Zhidomirov, G. M.; Yakovlev, A. L.; Milov, M. A.; Kachurovskaya, N. A.; Yudanov, I. V. *Catal. Today* **1999**, *51*, 397.
(33) Yakovlev, A. L.; Zhidomirov, G. M.; van Santen, R. A. *J. Phys. Chem. B* **2001**, *105*, 12297.
(34) Lewis, D. W.; Catlow, C. R. A.; Sankar, G.; Carr, S. W. *J. Phys. Chem.* **1995**, *99*, 2377.
(35) Feng, X.; Hall, W. K. *Catal. Lett.* **1997**, *46*, 11.
(36) Rice, M. J.; Chakraborty, A. K.; Bell, A. T. *J. Catal.* **1999**, *186*, 222.
(37) Rice, M. J.; Chakraborty, A. K.; Bell, A. T. *J. Catal.* **2000**, *194*, 278.
(38) Goodman, B. R.; Hass, K. C.; Schneider, W. F.; Adams, J. B. *Catal. Lett.* **2000**, *68*, 85.
(39) O'Malley, P. J.; Dwyer, J. *Zeolites* **1988**, *8*, 317.
(40) Alvarado-Swaisgood, A. E.; Barr, M. K.; Hay, P. J.; Redondo, A. *J. Phys. Chem.* **1991**, *95*, 10031.
(41) Redondo, A.; Hay, P. J. *J. Phys. Chem.* **1993**, *97*, 11754.
(42) Stave, M. S.; Nicholas, J. B. *J. Phys. Chem.* **1995**, *99*, 15046.
(43) Han, O. H.; Kim, C.-S.; Hong, S. B. *Angew. Chem., Int. Ed.* **2002**, *41*, 469.
(44) Olson, D. H.; Kokotailo, G. T.; Lawton, S. L. *J. Phys. Chem.* **1981**, *85*, 2238.
(45) Norman, J. G. Jr.; Ryan, P. B.; Noodleman, L. *J. Am. Chem. Soc.* **1980**, *102*, 4279.
(46) Noodleman, L.; Baerends, E. J. *J. Am. Chem. Soc.* **1984**, *106*, 2316.
(47) Noodleman, L.; Case, D. A. *Adv. Inorg. Chem.* **1992**, *38*, 423.
(48) Noodleman, L.; Peng, C. Y.; Case, D. A.; Mouesca, J. M. *Coord. Chem. Rev.* **1995**, *144*, 199.
(49) Noodleman, L. *J. Chem. Phys.* **1981**, *74*, 5737.
(50) Ruiz, E.; Alvarez, S.; Cano, J.; Polo, V. *J. Chem. Phys.* **2005**, *123*, 164110.
(51) Ruiz, E.; Cano, J.; Alvarez, S.; Alemany, P. *J. Comput. Chem.* **1999**, *20*, 1391.
(52) Yoshizawa, K.; Suzuki, A.; Yoshihito, S.; Yamabe, T. *Bull. Chem. Soc. Jpn.* **2000**, *73*, 815.
(53) Torrent, M.; Musaev, D. G.; Basch, H.; Morokuma, K. *J. Comput. Chem.* **2002**, *23*, 59.
(54) Becke, A. D. *Phys. Rev. A* **1988**, *38*, 3098.
(55) Lee, C.; Yang, W.; Parr, R. G. *Phys. Rev. B* **1988**, ***37***, 785.
(56) Treutler, O.; Ahlrichs, R. *J. Chem. Phys.* **1995**, *102*, 346.
(57) Zygmunt, S. A.; Mueller, R. M.; Curtiss, L. A.; Iton, L. E. *J. Mol. Struct. (THEOCHEM)* **1998**, *430*, 9.
(58) Yoshizawa, K.; Shiota, Y.; Yamabe, T. *J. Chem. Phys.* **1999**, *111*, 538.
(59) Zilberberg, I.; Gora, R. W.; Zhidomirov, G. M.; Leszczynski, J. *J. Chem. Phys.* **2002**, *117*, 7153.
(60) Furche, F.; Perdew, J. P. *J. Chem. Phys.* **2006**, *124*, 044103.
(61) Schäfer, A.; Huber, C.; Ahlrichs, R. *J. Chem. Phys.* **1994**, *100*, 5829.
(62) Ahlrichs, R.; Bär, M.; Häser, M.; Horn, H.; Kölmel, C. *Chem. Phys. Lett.* **1989**, *162*, 165.
(63) Gherman, B. F.; Baik, M.-H.; Lippard, S. J.; Friesner, R. A. *J. Am. Chem. Soc.* **2004**, *126*, 2978.
(64) Peters, B.; Heyden, A.; Bell, A. T.; Chakraborty, A. *J. Chem. Phys.* **2004**, *120*, 7877.
(65) Heyden, A.; Bell, A. T.; Keil, F. J. *J. Chem. Phys.* **2005**, *123*, 224101.
(66) Heyden, A. Theoretical investigation of the nitrous oxide decomposition over iron zeolite catalysts. Ph.D. thesis, Hamburg University of Technology, 2005.
(67) Choi, S. H.; Wood, B. R.; Ryder, J. A.; Bell, A. T. *J. Phys. Chem. B* **2003**, *107*, 11843.
(68) Choi, S. H.; Wood, B. R.; Bell, A. T.; Janicke, M. T.; Ott, K. C. *J. Phys. Chem. B* **2004**, *108*, 8970.
(69) Krishna, K.; Makkee, M. *Catal. Lett.* **2006**, *6*, 183.
(70) Slater, J. C. *Quantum Theory of Molecules and Solids. Volume 4: The Self-Consistent Field for Molecules and Solids*; McGraw-Hill: New York 1974.
(71) Vosko, S. J.; Wilk, L.; Nusair, M. *Can. J. Phys.* **1980**, *58*, 1200.
(72) Perdew, J. P.; Wang, Y. *Phys. Rev. B* **1992**, *45*, 13244.
(73) Kiwi-Minsker, L.; Bulushev, D. A.; Renken, A. *Catal. Today* **2005**, *110*, 191.
(74) Kurtz, D. M. *Chem. Rev.* **1990**, *90*, 585.
(75) Cornell, R. M. Schwertmann, U. *The Iron Oxides: Structure, Properties, Reactions, Occurrence and Uses*; VCH: Weinheim, Germany, 1996.